

AN ARTICULATED SWING ARM SYSTEM FOR SPHERICAL NEAR FIELD ANTENNA MEASUREMENTS AT MILLIMETER WAVE FREQUENCIES

ESA/ESTEC, NOORDWIJK, THE NETHERLANDS
6-9 OCTOBER 2015

Pieter N. Betjes, Daniël J. Janse van Rensburg, Stuart F. Gregson

Nearfield Systems Inc., 19730 Magellan Drive, Torrance, CA, 90502-1104, USA,
Email: pbetjes@nearfield.com / drensborg@nearfield.com / sgregson@nearfield.com

ABSTRACT

NSI has developed a high precision articulated swing arm system for millimeter wave spherical near-field measurements. This paper presents this system along with structural analysis and characterization, and explains what error corrections are performed in order to produce high accuracy results. Both simulated and measurements are shown to demonstrate the effectiveness of these correction measures.

1. INTRODUCTION

With increasing demand for integrated low directivity mm-wave antennas and on-chip devices, the need for accurate antenna pattern measurements on those antennas increases. Spherical near-field (SNF) testing is ideal for this sort of antenna as it samples the fields on a (almost) closed surface around the antenna under test (AUT). A complication is that the antennas call for low profile feeds, such as wafer probes, to avoid the need for an invasive, electromagnetically large connector in close proximity to the antenna. This imposes the additional requirement of measuring the antenna in an inertial frame of reference.

The NSI-700S-360 spherical near-field antenna measurement system was designed to accommodate these measurements. As the rigidity of the structure is bound by physical limitations, some positioning errors are expected, and these have been modelled and characterized ([1, 3]). In [2] and [3] it is shown that the radial error is the dominant error term which needs to be characterised and compensated for, and a first method to accomplish that is demonstrated, further results of which are shown in [4].

This paper describes a convenient way to model the radial error data for further use in antenna measurement error correction, allowing smart interpolation and some error filtering. Furthermore, a method to evaluate the effectiveness (and potentially to enhance that) of the radial error correction is introduced.

2. SYSTEM DESCRIPTION

Fig. 1 presents a schematic representation of the new SNF antenna test system. This system comprises a 500 mm diameter rotation stage mounted on a large floor stand and vertical tower. This positioner defines the horizontal ϕ -axis of rotation and is coincident and synonymous with the z -axis of the spherical measurement coordinate system. A second rotation stage is affixed to this stage at an angle of 90° to the ϕ -axis and this stage forms the θ -axis of a conventional right handed polar spherical coordinate system. A third rotary stage is attached to the θ -stage, again, at an angle of 90° only this time to the θ -axis and this third stage forms the χ -axis (*i.e.* polarisation axis). The combined motion of the ϕ and θ stages allows the probe tip to describe a path over the surface of a conceptual spherical surface centred about the intersection of those orthogonal axes and whose definition is in accordance with standard SNF theory. Crucially, and as is the case for conventional planar near-field measurements, data is acquired across a two-dimensional sampling interval with the AUT remaining entirely at rest for the duration of the measurement, a feature of particular importance when measuring very delicate probe-fed antennas which are prone to suffering changes in electrical excitation resulting from mechanical disturbances, *e.g.* vibration *etc.*.

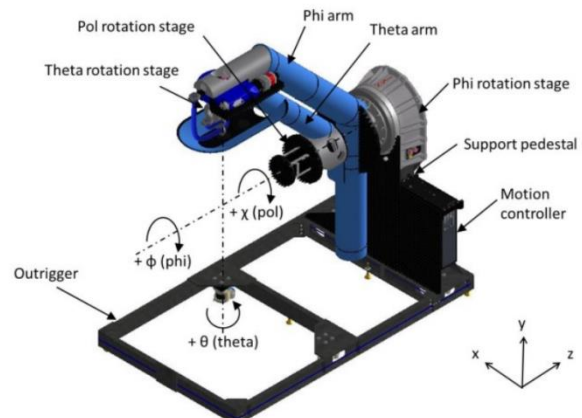


Figure 1, CAD rendering of the articulated spherical near-field antenna test system (NSI-700S-360) with associated measurement axes shown.

The NSI-700S-360 system is sufficiently large to incorporate mm-wave frequency up and down converter modules as part of the probe carriage assembly whilst maintaining a probe tip radius of approximately 500 mm, with the exact value depending upon the length of the specific mm-wave module and probe. The mm-wave modules are exchanged to cover the relevant waveguide frequency bands, leaving the remaining RF equipment rack and cabling portion of the RF sub-system intact, making for a convenient modular and upgradable test system that can span huge frequency ranges from a few GHz to sub mm-wave frequencies. Each of the rotation stages contain integrated RF rotary joints to maximize phase stability of the guided wave path across the sampling interval, with the ϕ -axis positioner also containing a multi channel slip-ring assembly for passing power and control lines to successive positioners. Figs. 2 and 3 show the SNF system at various θ and ϕ positions.



Figure 2, CAD rendering of NSI-700S-360 with probe at $(\theta, \phi) = (135^\circ, 0^\circ)$.

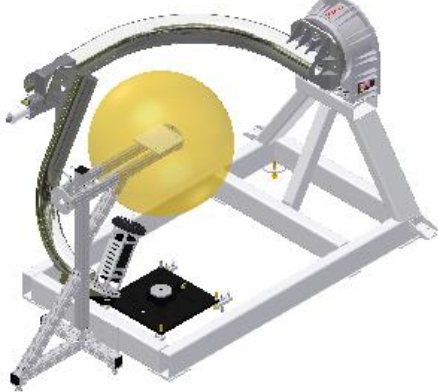


Figure 3, CAD rendering of NSI-700S-360 with probe at $(\theta, \phi) = (135^\circ, -90^\circ)$.

3. MODEL FOR RADIAL ERROR

As is the case for all antenna test systems, the NSI-700S-360 is subject to a range of potential error sources. Here, however, it has been shown that the radial

distance error is one of the more important terms within the facility level uncertainty budget [2, 3]. Thus, during the manufacture and installation of this class of system the radial error map is acquired and recorded using optical coordinate measuring instrumentation. Figs. 4, 5 and 6 present the radial error for three NSI-700S-360 systems with the data being presented in the form of a false colour checkerboard plot where the data is tabulated on a plaid monotonic and equally spaced spherical grid. The colour range denotes radial error between about -2 mm to +2mm.

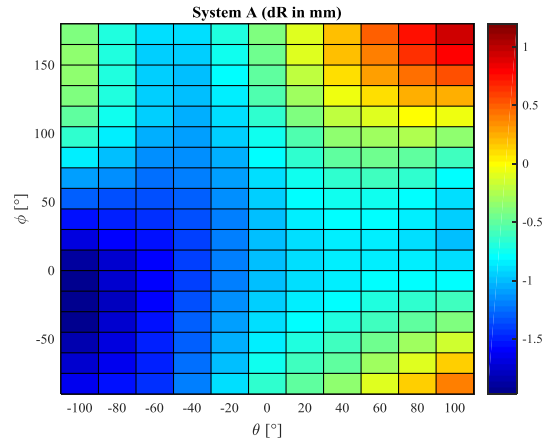


Figure 4, Radial error of System A as function of (θ, ϕ) .

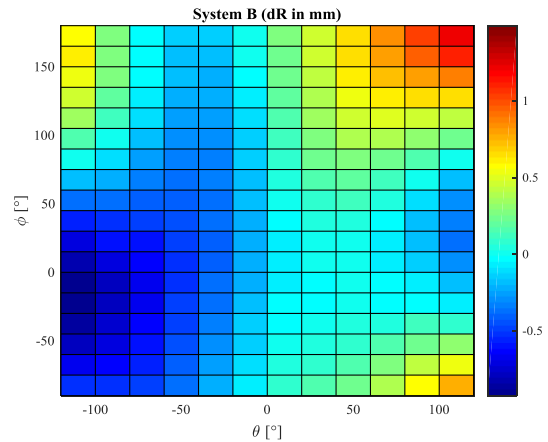


Figure 5, Radial error of System B as function of (θ, ϕ) .

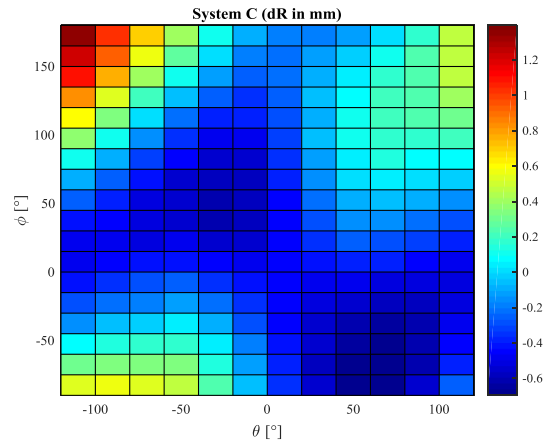


Figure 6, Radial error of System C as function of (θ, ϕ) .

From these figures it is clear that there is a common underlying behaviour of the radial error, especially for varying ϕ values. An even clearer representation of the behaviour of the error as a function of ϕ (for various θ -angles) is presented in Figure 7.

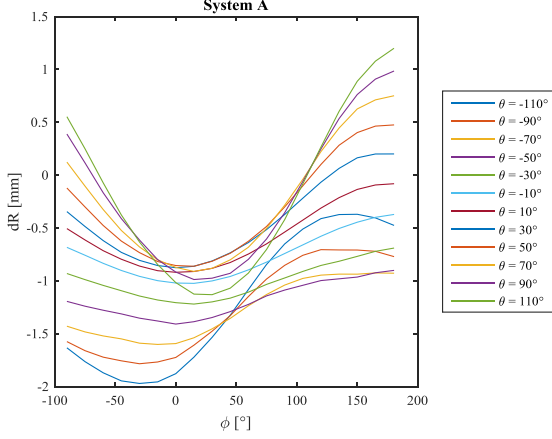


Figure 7, Measured radial error of system A as a function of ϕ for different values of θ .

Here, it is readily observed that the radial error behaves as a function of the spherical angles and can be modelled as

$$\delta R(\theta, \phi) = \delta R_0(\theta) + A(\theta) \sin(\phi - \phi_0(\theta)). \quad (1)$$

In order to determine the bias ($\delta R_0(\theta)$), amplitude ($A(\theta)$) and ϕ - offset ($\phi_0(\theta)$), this formula is rewritten as

$$\delta R(\theta, \phi) = \delta R_0(\theta) + A_s(\theta) \sin(\phi) + A_c(\theta) \cos(\phi), \quad (2)$$

which is a more convenient form for determining the coefficients $\delta R_0(\theta)$, $A_s(\theta)$ and $A_c(\theta)$. These coefficients can then be found by minimizing the RMS difference between the measured and the modelled data, using the formulation from Eq. 3 which is in accordance with the principle of least squares

$$\begin{pmatrix} A_s \\ A_c \\ \delta R_0 \end{pmatrix} = \begin{pmatrix} \sum K_i^2 & \sum K_i L_i & \sum K_i M_i \\ \sum L_i K_i & \sum L_i^2 & \sum L_i M_i \\ \sum M_i K_i & \sum M_i L_i & \sum M_i^2 \end{pmatrix}^{-1} \cdot \begin{pmatrix} \sum y_i K_i \\ \sum y_i L_i \\ \sum y_i M_i \end{pmatrix} \quad (3)$$

Here

$$\begin{aligned} K_i &= \sin(\phi_i) \\ L_i &= \cos(\phi_i) \\ M_i &= 1 \end{aligned} \quad (4)$$

After converting $A_s(\theta)$, $A_c(\theta)$ to $A(\theta)$ and $\phi_0(\theta)$ using common trigonometric identities, for the mechanical system in our example this results in the parameters as shown in Figure 8.

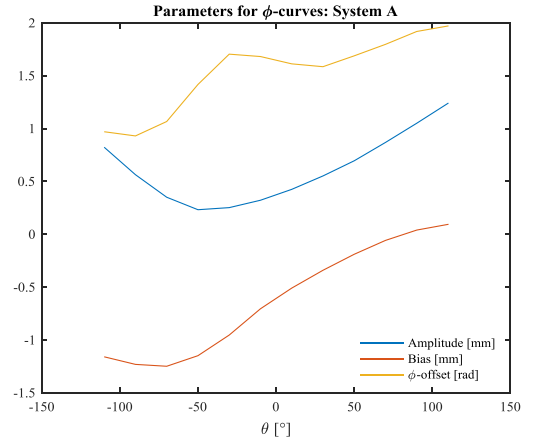


Figure 8, Parameters for the radial error vs ϕ curves as a function of θ .

The radial errors can therefore be modelled using these parameters. The result is shown in Figure 9, which can be compared directly to Fig. 7.

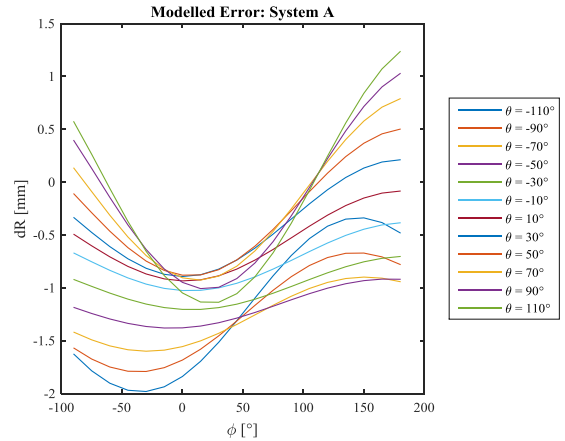


Figure 9, Modelled radial error of system A as a function of ϕ for different values of θ , using parameters from Figure 8.

The residual error (*i.e.* difference between measured and this modelled radial error) is shown in Figure 10.

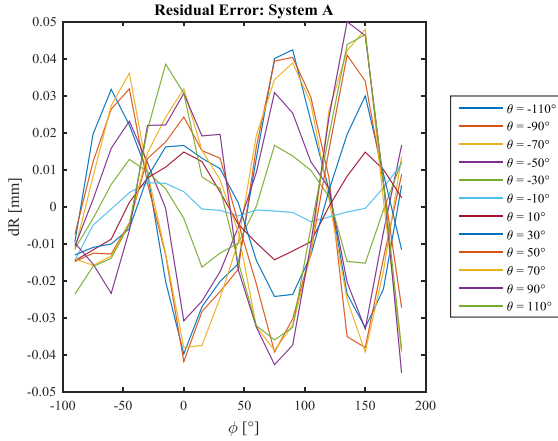


Figure 10, Residual error (difference between measured radial error and modelled radial error) as a function of ϕ for different values of θ .

This analysis was performed for the three systems shown here and in all instances residual errors were found to be within a ± 0.05 mm bracket. The curves depicted in Fig. 10 represent a worst case, indicating that the underlying functional form remains consistent across the various systems.

SNF measurements require data to be taken precisely and accurately on a raster grid at (θ, ϕ) positions that are dictated by the frequency and the shape, size and location of the device under test. As these parameters will vary, it is not practical to perform deformation characterization at each and every possible (θ, ϕ) position to be used. As such, the modelling approach presented here for the mechanical data is needed in order to efficiently compensate measured data. The modelling as introduced has the benefit that instead of using generic interpolation [5] of a relatively coarse grid of measured mechanical data, *e.g.* with the use of generic piecewise polynomial interpolation, radial errors are now calculated from a model that has a natural link to the topology of the mechanical system, and the parameters of which are still based on actual mechanical measurements. The fact that the parameters in this model are determined using the principle of least squares minimizes the impact of random errors and localised noise. Thus, some filtering of the mechanical data is inherently included.

4. ELECTRICAL VERIFICATION

After having modelled the radial error (a radial error can now be calculated at every ϕ -position using Eq. 1 and properly interpolating the parameter curves, *cf.* those shown in Figure 8), the radial error characterization can now be used to compensate the phase of spherical near-field antenna measurements [1, 4]. For this, the radial error for the applicable (θ, ϕ) position is multiplied by the wavenumber and subtracted from the measured phase to provide a first order correction for the

imperfections in the spherical sampling surface. Typically, SNF antenna measurements have some inherent redundancy, and often a θ -cut is recorded for ϕ -values which are displaced by 180° (typically the first and last cut of a measurement). These cuts can be used to perform a self-alignment of the mechanical system (see [6]). This method can also be applied to verify the effectiveness of the radial error correction as presented here. Figure 11 and Figure 12 demonstrate this for a measurement taken on System A. Figure 11 shows the differences of the phase of the θ -cuts at the first and last ϕ -position (in red) and the curve of the associated error model (in blue) before applying the radial error compensation, showing a corresponding non-intersection error of 0.6 mm. At the frequency of the shown measurement (110 GHz), this would correspond to a non-intersection error of almost 80° of phase, which would render this measurement severely compromised. After applying the compensation (curves shown in Figure 12), the corresponding non-intersection error is reduced to 0.05 mm (7.13° of phase at 110 GHz), which makes this a very perfectly acceptable near-field measurement.

It should be noted that the large excursions at the edges of the red curves in Figure 11 and Figure 12 are due to the low levels of the amplitudes in those directions.

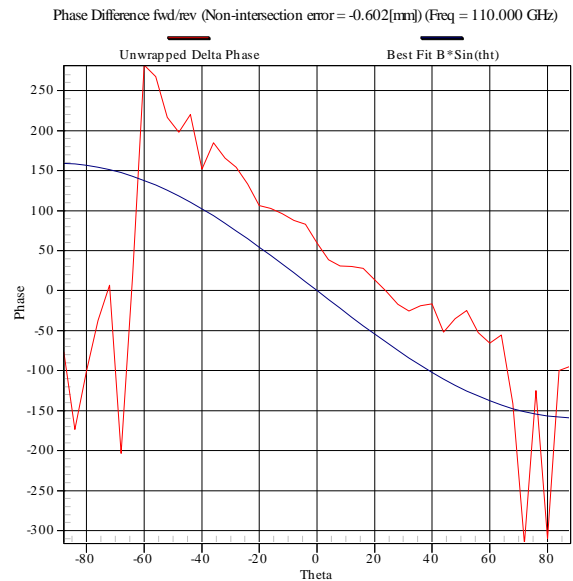


Figure 11, Non-intersection assessment prior to compensation of the radial error.

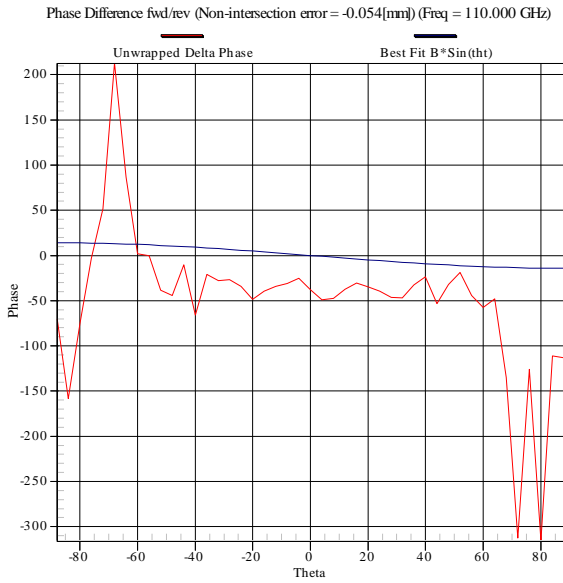


Figure 12, Non-intersection assessment after compensation of the radial error.

The presented assessment method can be expanded to cover multiple ϕ -positions, so that a rigorous health check (and possibly even a self-correction) of the system can be done without the need to set up an optical measurement instrument.

5. ANTENNA MEASUREMENT RESULTS

As a final verification of the effectiveness of the modelled data and position correction algorithm, actual processed SNF measurements are shown in Figure 13 and Figure 14. Here, the phase correction resulting from the modelled interpolation is shown side by side with the results of the conventional phase correction (using direct piecewise polynomial interpolation of the radial error data) as presented in [2], as well as no phase correction at all. Fig. 13 shows the principal plane radiation patterns for a horn antenna measured at 110 GHz and Fig. 14 shows the orthogonal plane cut. In both instances the SNF data corrected in phase for radial distance variation, are markedly improved in contrast to the uncorrected case. However, both interpolated correction approaches seem to perform well and provide results that are indistinguishable (blue and red curves). It can be stated that the modelling approach presented here provides a robust and efficient interpolation scheme that allows for calculation of radial distance phase correction on any SNF sampling grid. The method should be less sensitive to the effects of random measurement errors within the optical coordinate measurement grid.

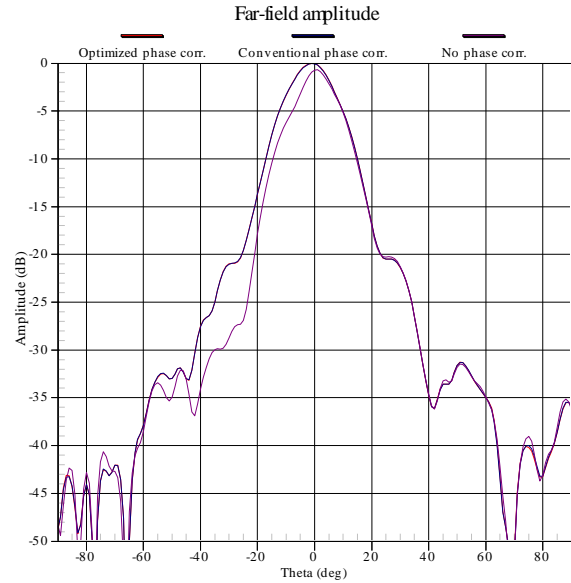


Figure 13, Comparison between correction based on the modelled radial error, correction based on the directly interpolated radial error and no correction ($\phi=0^\circ$).

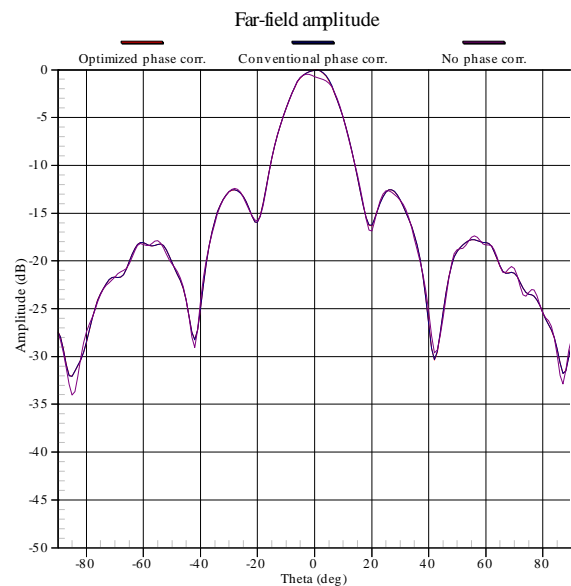


Figure 14, Comparison between correction based on the modelled radial error, correction based on the directly interpolated radial error and no correction ($\phi=90^\circ$).

6. CONCLUSIONS AND RECOMMENDATIONS

An effective way to model (and therefore to interpolate) radial error measurements on an NSI-700S-360 was presented, along with an effective evaluation method. It was shown that using the error data results in good final results for processed antenna measurement data at 110 GHz and a way to improve the spherical alignment of the system.

It is intended to implement an extended health-check verification method based on the spherical alignment method as described in [6]. Also, further investigation into the behaviour of the parameters as a function of θ -angle is planned, with the possibility that this eventually will give more accurate and/or easier to obtain (radial) error data for the NSI-700S-360 system.

7. ACKNOWLEDGEMENT

The authors would like to acknowledge Dan Swan and Karl Haner for the mechanical characterizations, and Pat Pelland for RF measurements.

8. REFERENCES

1. Janse van Rensburg, D. & Gregson, S. (2014). Parametric Study of Probe Positioning Errors in Articulated Spherical Near-field Test Systems for mm-Wave Applications. IEEE Conference on Antenna Measurements & Applications, Antibes Juan-les-Pins (France), 16-19th Nov. 2014.
2. Janse van Rensburg, D. (2015). Factors limiting the upper frequency of mm-wave spherical near-field test systems. EUCAP 2015, Lisbon (Portugal), 12 – 17 April 2015.
3. Janse van Rensburg, D. & Wynne, J. (2012). Parametric Study of Probe Positioning Errors in Spherical Near-field Test Systems for mm-Wave Applications. IEEE APS/URSI, Conference Chicago, 2012.
4. Janse van Rensburg, D. & Betjes, P (2015). Structural Correction of a Spherical Near-Field Scanner for mm-Wave Applications. AMTA 37th Annual Meeting & Symposium, Long Beach, California (USA), 11-16 Oct, 2015
5. Gregson, S.F., McCormick J, Parini, C.G. (2007). *Principles of Planar Near-Field Antenna Measurements*, IET Press, ISBN 978-0-86341-736-8.
6. Newell, A.C. & Hindman, G. (1997). The Alignment of a Spherical Near-Field Rotator Using Electrical Measurements. AMTA 19th Annual Meeting & Symposium, November 1997